Biocatalysis and Agricultural Biotechnology 17 (2019) 566–570

Contents lists available at ScienceDirect

Biocatalysis and Agricultural Biotechnology

journal homepage: www.elsevier.com/locate/bab

Investigation on growth and morphology of *in vitro* generated struvite crystals

Muhammed A.P. Manzoor[a,c], M. Mujeeburahiman[b], Surya Ram Duwal[a], P.D. Rekha[a,*]

[a] Yenepoya Research Centre, Yenepoya University, Mangalore, Karnataka 575018, India
[b] Department of Urology, Yenepoya Medical College, Yenepoya University, Mangalore, Karnataka 575018, India
[c] ICAR–Indian Institute of Spices Research, Kozhikode 673012, Kerala, India

ARTICLE INFO

Keywords:
Struvite
Kidney stone
Crystallization
pH
Morphology
Characterization

ABSTRACT

Struvite stones develop as a result of urinary tract infections by urease-producing bacteria. Here, we report the dynamics of *in vitro* crystallization of struvite at various pH using single diffusion gel growth technique. Sodium metasilicate gel and ammonium dihydrogen phosphate were used as a medium for growing the struvite crystals. The composition, crystalline nature, and surface morphology of the crystals were studied using FTIR spectroscopy, XRD, TGA, DSC, and SEM. The struvite crystals displayed different morphologies like dendritic, envelope and rectangular shapes at different pH. Crystal faces were different at opposite ends of the crystallographic axis of the struvite crystals. Large X-shaped crystals with dendritic growth having main trunk and branches were observed. SEM revealed the porous internal structure of struvite. The results indicate that pH has a significant effect on the morphology and growth of struvite crystals. The present study will provide evidence for the importance of pathological bio-mineralization and/or crystallization.

1. Introduction

Kidney stones form as a result of supersaturation of urine and their formation depends mainly on urinary pH, ionic strength, specific gravity and concentration of solutes of urine (Ratkalkar and Kleinman, 2011). The incidence of kidney stone is increasing globally and it depends mainly on geography and environmental conditions. Lifestyle factors, genetic and dietary habits are also established risk factors for kidney stone disease (Saxena and Sharma, 2010).

Struvite (Magnesium ammonium phosphate hexahydrate, $MgNH_4PO_4{\cdot}6H_2O$) or infection stone makeup approximately 10–15% of all stones worldwide and develop as a result of urinary tract infections by urease-producing microorganism(s) with high recurrence rate (Flannigan et al., 2014; Manzoor et al., 2018a). The bacterial enzyme urease can cause super-saturation of PO_4^{3-} and form crystallization of struvite. The struvite crystal formation is represented by the following reaction;

$$Mg^{2+} + NH_4^{+} + PO_4^{3-} + 6H_2O \rightarrow MgNH_4PO_4{\cdot}6H_2O$$

Among all stone types; only struvite can form staghorn, and result in complications like pyonephrosis, and damage the epithelium of the internal renal walls, resulting in loss of kidney function (Prywer and Torzewska, 2010; Chauhan et al., 2008a; Manzoor et al., 2018b). Our previous report shows a high diversity of mixed stones among Indian population and struvite was one of the major compositions either as pure or mixed type's calculi (Manzoor et al., 2017, 2018c). In addition, there is a need for understanding the bacterial association in stone, and its associated complications (Manzoor et al., 2018d; Shabeena et al., 2018).

Crystallization and morphogenesis of struvite have been extensively investigated (Chauhan and Joshi, 2008b; Prywer et al., 2012; Li et al., 2015). Struvite can form various crystal habits such as staghorn-like dendritic morphologies, X-shaped and unusual tabular morphologies (Prywer and Torzewska, 2010; Manzoor et al., 2018a). Morphological variations of struvite crystals may depend on various factors such as supersaturation, growth kinetics, pH, specific gravity, and the effect of modulators (Prywer and Torzewska, 2010). The preferred pH for struvite crystallization is 7.2. The super-saturation is the driving force for crystallization, and urinary pH tends to change with diet. Moreover, little is known about the morphology of *in vitro* generated struvite at various pH. Urinary pH is one of the important factors for the formation of struvite crystals and hence, we investigated the growth, morphology, and habit of struvite using single diffusion gel growth technique at various pH. The crystals were characterized using Fourier transform infrared (FTIR) spectroscopy, X-ray diffraction (XRD), thermogravimetric analysis (TGA), differential scanning calorimetry (DSC), and

* Corresponding author.
E-mail address: dydirectoryrc@yenepoya.edu.in (P.D. Rekha).

https://doi.org/10.1016/j.bcab.2019.01.023
Received 8 December 2018; Received in revised form 9 January 2019; Accepted 11 January 2019
Available online 14 January 2019
1878-8181/

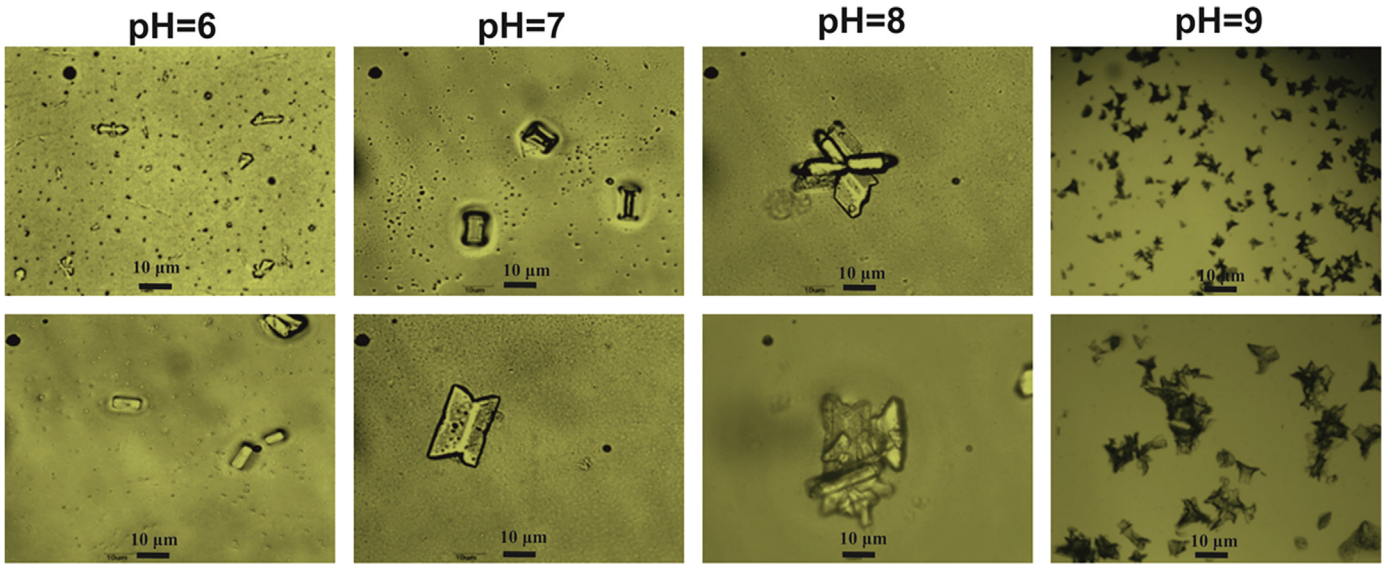

Fig. 1. Microscopic images showing struvite crystals grown at different pH.

Scanning electron microscopy (SEM) to study the possible differences.

2. Materials and methods

2.1. Synthetic urine preparation

The synthetic urine used for crystallization was prepared according to Griffith et al. (1976) (g/L): $CaCl_2{\cdot}2H_2O$: 0.651; $MgCl_2{\cdot}6H_2O$: 0.651; NaCl: 4.6; KH_2PO_4: 2.8; Na_2SO_4, 2.3; KCl, 1.6; NH_4Cl, 1.0; sodium citrate, 0.65; sodium oxalate, 0.02; urea, 25.0; creatine, 1.1. The pH of the synthetic urine was adjusted to 7.0 before crystallization experiments.

2.2. Crystallization experiments

Single diffusion gel technique was adopted for the growth of struvite crystals as described elsewhere (Manzoor et al., 2018b). Briefly, sodium metasilicate solution of specific gravity 1.05 was used to prepare the gel. An aqueous solution of ammonium di-hydrogen phosphate (0.5 M) was mixed with the sodium metasilicate solution in an appropriate volume so that the pH of 7.0 was achieved. After the gelation, 20 mL supernatant solution of 0.5 M magnesium acetate in synthetic urine was gently poured on the gels without disturbing the gel. The supernatant pH was adjusted to 6, 7, 8 and 9 to study the crystal growth of the struvite in these pH.

The following reaction is expected to occur in the gel between the two reactants;

$$NH_4H_2PO_42H_2O + (CH_3COO)_2\ Mg{\cdot}4H_2O \rightarrow NH_4MgPO_4{\cdot}6H_2O + 2CH_3COOH$$

All the experiments were performed under triplicate in aseptic conditions at the temperature of 37 ± 0.5 °C. After 20 days, the well-grown crystals were harvested by decanting the test tubes carefully. The crystals harvested were dried and stored for further analysis.

2.3. Characterization of struvite crystals

The preliminary morphology of the crystals was recorded using stereomicroscope (Carl Zeiss, Göttingen, Germany). It was further characterized by FTIR spectroscopy, XRD, TGA, DSC and SEM. For FTIR spectroscopy, the powdered crystals (approx. 10 mg) were directly placed in the instrument (Shimadzu IR Prestige-21) and spectra were recorded at mid-frequency range (4000–400 cm^{-1}) at 4 cm^{-1} resolution. From the IR spectra the major peaks were identified. The XRD measurements were performed with a Rigaku MiniFlex 600 laboratory diffractometer. Diffraction patterns were registered within the 2θ angle range of 10–60°. The other parameters included, Cu-Kα radiation (λ = 1.5406 Å) working at 40 kV, 15 mA. Temperature was set to 22 ± 1 °C using a Na (Ti) I scintillation counter. Phase identifications were measured from the diffraction peaks as previously described (Stefov et al., 2004; Cahil et al., 2007; Dřínek et al., 2015; Sindu et al., 2017; Vasantharaj et al., 2018). Crystalline phases were identified based on the JCPDS database. The TGA, and DSC were performed simultaneously using SDT Q600 V20.9 Build 20 instrument. The analysis was performed with 20 mg sample under the nitrogen atmosphere between at temperature 27–700 °C and at a scanning rate of 10 °C/min.

The microstructure and morphology of crystals were observed using SEM. For this, the samples were separately sputter-coated with gold (Au) and observed using SEM (Carl Zeiss, Germany). Micrographs were recorded from different regions of the stone 1000–10000 X amplification was used to analyze the microstructure.

3. Results and discussion

The initial experiment revealed the early stages of struvite crystallization at different pH. During this period, the size of crystals varied from a few microns to more than 10 µm with distinct structure (Fig. 1). Struvite crystallization was found to be possible within the range of pH 6–7.5 in the gel method (Chauhan and Joshi, 2014). Figs. 2 and 3 shows the morphology of struvite crystals at different pH. Struvite crystals in the gel media mainly exhibit a coffin-like habit with well-defined planes which further exhibit X-shaped dendrite crystals. These characteristic hemimorphic habits and morphology were reported previously in detail (Li et al., 2015; Manzoor et al., 2018a). The crystals were mainly transparent, and/or translucent. We also observed the morphologic differences in the struvite crystals formed at the top and bottom layers of the gel in the test tube. The depth of crystal formation was dependent on the availability of the minerals as well as the pH of the supernatant in the gel medium. All the dendritic, envelope and rectangular like shapes were confirming to pure struvite. At pH 7.2, transparent prismatic crystals with an approximate size of 6 mm were formed at higher depth from the gel-liquid interface at the end of 10th day. Moreover, the transparency of the struvite crystal gradually decreased with the increasing pH of the supernatant solution. Above pH 7.2, the structure changed from a distinctly box-like network to a structure of loosely bound platelets. The sizes of the grown struvite crystals became

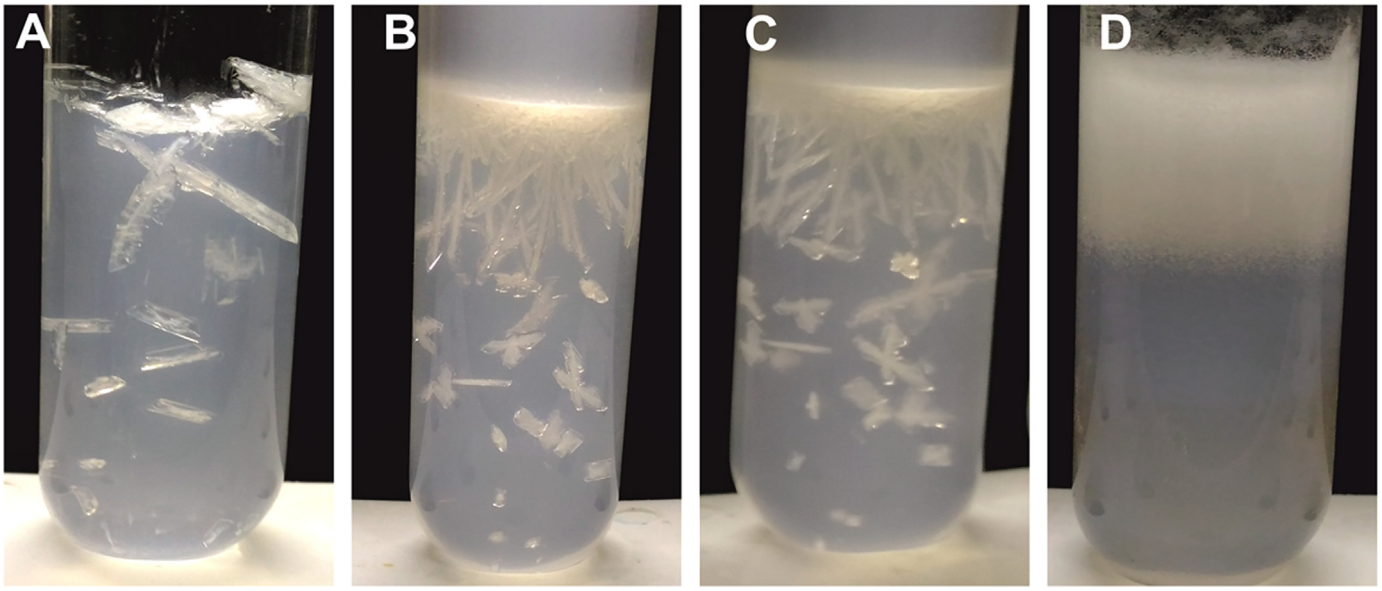

Fig. 2. Photograph of the struvite crystals grown in gel medium in test tubes at different pH (A) pH:6, (B) pH:7, (C) pH:8, (D) pH:9.

gradually smaller when the depth of the gel column increased from the gel–liquid interface. Poly-crystals form as a result of diffusion of the magnesium acetate from the supernatant solution which increases the supersaturation (Chauhan and Joshi, 2014).

In the present study we observed that the *in vitro* struvite crystals can be formed in the pH range of 6–9. The crystal habit is variable according to initial pH of the gel supernatant solution. Crystals developed at pH 6 were mainly spherical, and at pH 7, they were mainly coffin-like morphology. Large X-shaped and unusual tabular struvite forms were also found in pH 7. At pH 8, twinned elongated crystals were observed in addition to the X-shaped crystals. At pH 9, the struvite crystals were mainly hopper like structure and were mainly coexisting with dendrite-like crystals.

The struvite crystals showed characteristic IR absorption peaks at 1469, 1435 and 1400 cm^{-1} attributed to (v4) NH_4^+ antisymmetric bending. The main peak at 1010 cm^{-1} was due to the absorption of PO_4^{3-} mode antisymmetric stretch. Other peaks present were at 892 and 761 cm^{-1} of ammonium-water H bonding and water-water H bonding and peaks at 572 and 462 cm^{-1} assigned to P-O bend and the PO_4^{3-} modes respectively (Fig. 4a). FTIR pattern of struvite crystals grown in the gel medium is in accordance with the values reported in the literature (Frost et al., 2004, 2005; Saidou et al., 2009).

The XRD analysis revealed the appearance of struvite crystals in orthorhombic Pmn21 space group (cell parameters: a = 6.955 Å, b = 11.2 Å, c = 6.142 Å). The XRD patterns for the dendritic, envelope and rectangular like shapes of crystals were similar and the representative XRD pattern is given in Fig. 4b. All the diffraction peaks were well indexed as struvite without any traces of other impurity phases. The struvite exhibits increased peak intensity corresponding to (020) as well as (111) planes. XRD pattern of struvite crystals grown in the gel medium are identical with that reported in the literature (Bindhu et al., 2015; Manzoor et al., 2018a, 2018b).

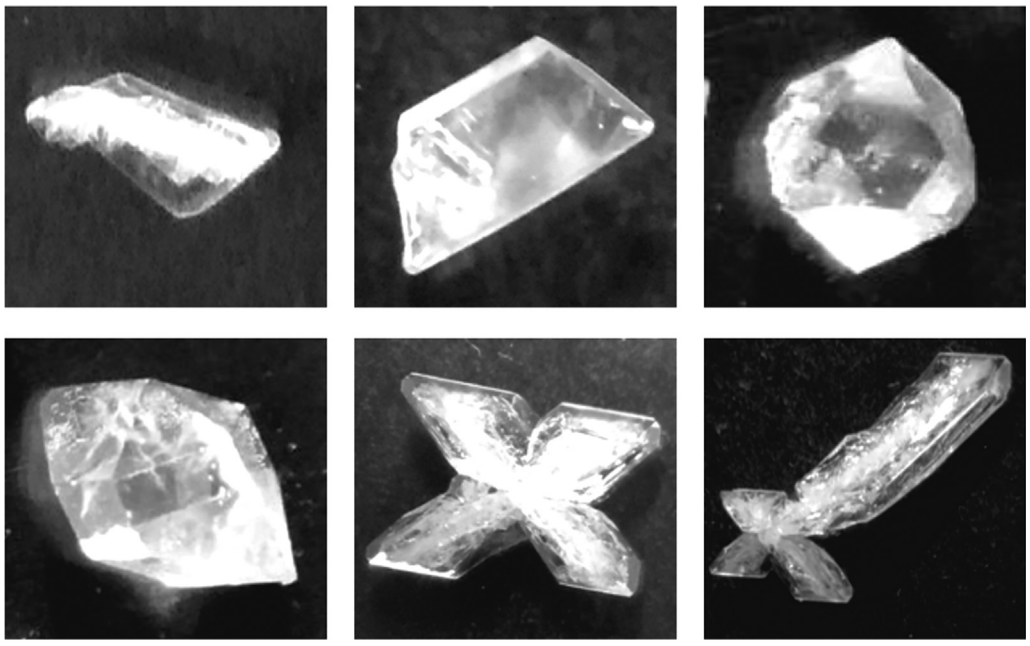

Fig. 3. Different morphology of struvite crystals grown *in vitro* using single diffusion gel growth technique.

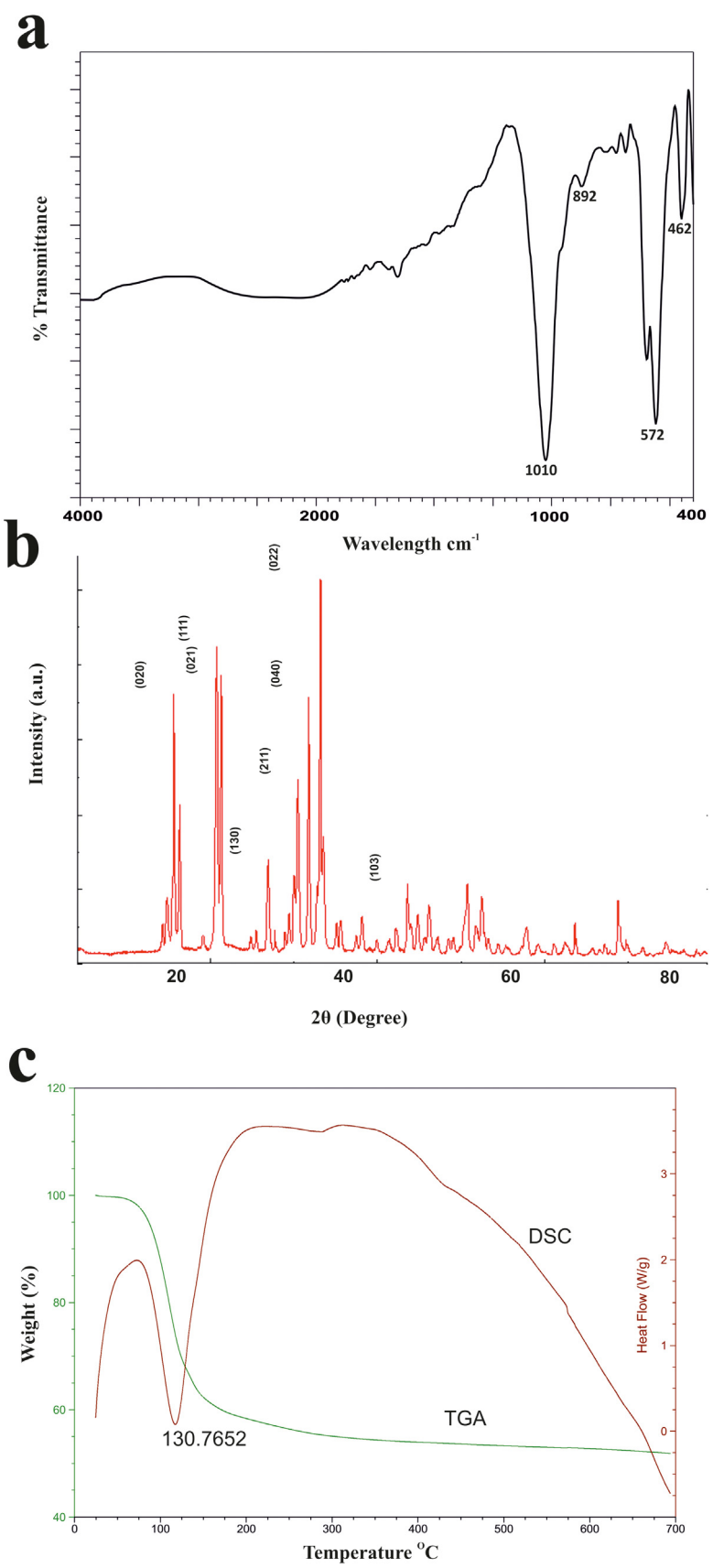

Fig. 4. (a) Representative FTIR spectra of the of the grown struvite crystal. (b) XRD pattern of the of the grown struvite crystal. (c) TGA and DSC profiles of struvite crystal generated *in vitro* (pH 7).

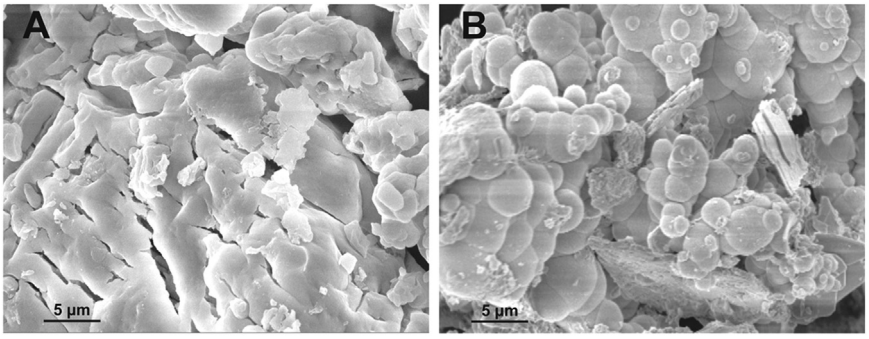

Fig. 5. SEM analysis of struvite crystals revealing the porous structure (pH 7).

Fig. 4c shows the TGA and DSC analysis of struvite crystals recorded in the temperature range 27–700 °C at the rate of 10 °C/min. The initial loss in the weight is due to the dehydration of struvite crystals and at 700 °C, 67.54% of original weight was retained. The TGA study confirmed the identity of struvite crystals grown in the gel medium as reported in the literature (Frost et al., 2004). The DSC curve exhibited one main endothermic peak at 130.76 °C, which is suggesting the maximum weight loss at this temperature (Fig. 4c).

Morphology and texture of struvite crystals were further studied by SEM. The microscopy images revealed that the single struvite crystals have well-defined faces and these crystals are constructed from multi-layered depositions. The porous nature of struvite can be easily identified in the struvite crystals (Fig. 5). These multi-layered depositions are commonly observed during the formation of struvite crystals *in vitro* in the presence of natural compounds (Bindhu et al., 2015).

4. Conclusion

Struvite crystallization was affected by pH with the most favourable pH for crystallization being in the range of 7–8. Though the crystallization was not affected by the supernatant pH, but the morphology of the stones was different particularly at lower to higher pH. In conclusion, pH has a significant effect on the morphology of the struvite crystals. Although, further studies are warranted to understand the role of pH on crystallization of struvite to understand various biotechnological processes from a different perspective.

References

Bindhu, B., Swetha, A.S., Veluraja, K., 2015. Studies on the effect of *Phyllanthus emblica* extract on the growth of urinary type struvite crystals *in vitro*. Clin. Phytosci. 1, 3.
Cahil, A., Najdoski, M., Stefov, V., 2007. Infrared and Raman spectra of magnesium ammonium phosphate hexahydrate (struvite) and its isomorphous analogues. IV. FTIR spectra of protiated and partially deuterated nickel ammonium phosphate hexahydrate and nickel potassium phosphate hexahydrate. J. Mol. Struct. 834, 408–413.
Chauhan, C.K., Joseph, K.C., Parekh, B.B., Joshi, M.J., 2008a. Growth and characterization of struvite crystals. Ind. J. Pure Appl. Phys. 46, 507–512.
Chauhan, C.K., Joshi, M.J., 2008b. Growth inhibition of Struvite crystals in the presence of juice of *Citrus medica* Linn. Urol. Res. 36, 265–273.
Chauhan, C.K., Joshi, M.J., 2014. Growth and characterization of struvite-Na crystals. J. Cryst. Growth 401, 221–226.
Dřínek, V., Klementová, M., Fajgar, R., Dytrych, P., 2015. Silicon nanowires grown on metal substrates via self-catalyst mechanism. Mater. Chem. 160, 109–112.
Flannigan, R., Choy, W.H., Chew, B., Lange, D., 2014. Renal struvite stones -pathogenesis, microbiology, and management strategies. Nat. Rev. Urol. 11, 333–341.
Frost, R., Weier, M., Erickson, K., 2004. Thermal decomposition of struvite. J. Therm. Anal. Calorim. 76, 1025–1033.
Frost, R.L., Weier, M.L., Martens, W.N., Henry, D.A., Mills, S.J., 2005. Raman spectroscopy of newberyite, hannayite and struvite. Spectrochim. Acta 62, 181–188.
Griffith, D.P., Musher, D.M., Itin, C., 1976. Urease. The primary cause of infection-induced urinary stones. Invest Urol. 13, 346–350.
Li, H., Yao, Q.Z., Wang, Y.Y., Li, Y.L., Zhou, G.T., 2015. Biomimetic synthesis of struvite with biogenic morphology and implication for pathological biomineralization. Sci. Rep. 5, 7718. https://doi.org/10.1038/srep07718.
Manzoor, M.A.P., Mujeeburahiman, M., Rekha, P.D., 2017. Association of serum biochemical panel with mineralogical composition of kidney stone in India. Acta Med. Int. 4, 26–30.
Manzoor, M.A.P., Singh, B., Agrawal, A.K., Arun, A.B., Mujeeburahiman, M., Rekha, P.D., 2018a. Morphological and micro-tomographic study on evolution of struvite in synthetic urine infected with bacteria and investigation of its pathological biomineralization. PLoS One 13 (8), e0202306.
Manzoor, M.A.P., Duwal, S.R., Mujeeburahiman, M., Rekha, P.D., 2018b. Vitamin C inhibits crystallization of struvite from artificial urine in the presence of *Pseudomonas aeruginosa*. Int. Braz. J. Uro. 44, 1234–1242.
Manzoor, M.A.P., Mujeeburahiman, M., Rekha, P.D., 2018c. Electron probe micro-analysis reveals the complexity of mineral deposition mechanisms in urinary stones. Urolithiasis 46, 1–12.
Manzoor, M.A.P., Shabeena, K.S., Mujeeburahiman, M., Khan, A., 2018d. In dwelling J ureteral stents associated asymptomatic bacteraemia caused by multidrug resistant strain of *Kocuria kristinae*. J. Clin. Diagn. Res. 12, 15–16.
Prywer, J., Torzewska, A., 2010. Biomineralization of struvite crystals by Proteus mirabilis from artificial urine and their mesoscopic structure. Cryst. Res. Technol. 45, 1283–1289.
Prywer, J., Torzewska, A., Płociński, T., 2012. Unique surface and internal structure of struvite crystals formed by *Proteus mirabilis*. Urol. Res. 40, 699–707.
Ratkalkar, V.N., Kleinman, J.G., 2011. Mechanisms of stone formation. Clin. Rev. Bone Miner. Metab. 9, 187–197.
Saidou, H., BenMoussa, S., BenAmor, M., 2009. Influence of airflow rate and substrate nature on heterogeneous struvite precipitation. Environ. Technol. 30, 75–83.
Saxena, A., Sharma, R.K., 2010. Nutritional aspect of nephrolithiasis. Indian J. Urol. 26, 523–530.
Shabeena, K.S., Bhargava, R., Manzoor, M.A.P., Mujeeburahiman, M., 2018. Characteristics of bacterial colonization after indwelling double-J ureteral stents for different time duration. Urol. Ann. 10, 71–75.
Sindu, P.A., Kolanthai, E., Suganthi, R.V., Arul, K.T., Manikandan, E., Catalani, L.H., Kalkura, S.N., 2017. Green synthesis of Si-incorporated hydroxyapatite using sodium metasilicate as silicon precursor and *in vitro* antibiotic release studies. J. Photochem. Photobiol. B 175, 163–172.
Stefov, V., Šoptrajanov, B., Spirovski, F., Kuzmanovski, I., Lutz, H.D., Engelen, B., 2004. Infrared and Raman spectra of magnesium ammonium phosphate hexahydrate (struvite) and its isomorphous analogues. I. Spectra of protiated and partially deuterated magnesium potassium phosphate hexahydrate. J. Mol. Struct. 689, 1–10.
Vasantharaj, S., Sripriya, N., Shanmugavel, M., Manikandan, E., Gnanamani, A., Senthilkumar, P., 2018. Surface active gold nanoparticles biosynthesis by new approach for bionanocatalytic activity. J. Photochem. Photobiol. B 179, 119–125.